# **NURETH14-282**

# EFFECT OF WALL BOUNDARY CONDITION ON SCALAR TRANSFER IN TURBULENT LOW-PRANDTL-NUMBER CONVECTION

# Ivan Otic and Xu Cheng

Karlsruhe Institute of Technology
Institute for Fusion and Reactor Technologies
Kaiserstrasse 12, 76131 Karlsruhe, Germany
ivan.otic@kit.edu, xu.cheng@kit.edu

#### **Abstract**

One important issue in understanding and modeling of turbulent heat transfer is the behavior of the fluctuating temperature and velocity close to the wall. The usual approach assumes the temperature fluctuations to be zero on the wall. This assumption of ideal heat flux wall boundary condition may result in the ill-posedness of the energy equation as discussed by Sommer et al. 1994. In the present paper constant heat flux boundary condition was assumed, allowing nonzero wall temperature fluctuations and the effects of temperature fluctuations close to the wall are investigated using the LES simulation approach. The subgrid-scale (SGS) turbulence model for non-unity Prandtl numbers by Otic, 2010 is applied to analyze forced convection in a channel at friction velocity-based Reynolds numbers 390 and 599, for Prandtl numbers 0.701 and 0.022. A simple criteria for the contribution of turbulence models to the resolved scales in the entire computational domain is provided. Simulation data is statistically analyzed and compared with the DNS results from the literature.

## Introduction

Turbulent forced convection in liquid metal cooled nuclear reactors is of fundamental interest. One important issue in understanding and modeling of turbulent heat transfer is the behavior of the fluctuating temperature and velocity close to the wall. Common DNS approach is to consider the system as fully developed while the wall boundary condition of ideal heat flux is applied, i.e. the temperature fluctuations are assumed to be zero on the wall. This assumption of ideal heat flux wall boundary condition may result in the ill-posedness of the energy equation as discussed by Sommer  $et\ al.$  [1]. Tiselj  $et\ al.$  [2] performed direct numerical simulation of fully developed turbulent velocity and temperature fields in a flume, for friction velocity-based Reynolds number of 171 and Prandtl number Pr=1.0 using isoflux wall boundary condition which allows a non-zero temperature fluctuations on the wall. Tiselj and colleagues compared their results with the DNS by Kawamura  $et\ al.$  [3] where the ideal heat flux boundary condition is applied and found that the profile of the mean temperature was not affected by the type of heat flux boundary condition (BC). However, they also found that the type of heat flux BC has a profound effect on the statistics of the

temperature fluctuations in the near-wall region. In the case where thermal conductivity of wall and fluid are strongly different ideal heat flux BC may reflect the physical mechanisms of turbulent convection correctly. If thermal conductivity of walls and fluid are similar as in the case of liquid metal convection the ideal heat flux wall boundary condition may be insufficient. In addition the assumption of zero temperature fluctuations at the walls can not explain the thermal streaks on the wall.

For nuclear engineering and design computational fluid dynamics (CFD) codes are commonly applied. CFD calculations usually apply statistical turbulence closures based on Reynolds-averaged Navier-Stokes (RANS) equations. For RANS modeling the similarity of velocity and temperature over all scales is assumed and statistical turbulent Prandtl number models or algebraic heat flux models based on the turbulent kinetic energy and its dissipation rate are commonly applied. In this case the problem is twofold: *a)* Possibly incorrect wall boundary condition; *b)* The noslip boundary condition for the velocity induce vanishing temperature fluctuations near the walls. Same deficiencies may occur for the near wall approximations applied to LES.

Analysis, development and validation of turbulence models require turbulence data provided from experiments and detailed numerical simulations like large eddy simulation (LES) or direct numerical simulation (DNS). In large eddy simulation, the three-dimensional time dependent large scale field is computed directly from the filtered equations and the effects of the small unresolved scales are modeled. The severe Reynolds number restriction in direct numerical simulations (DNS), is largely reduced in LES. This advantage is obtained at the expense of modeling the small scales, the so called subgrid scales (SGS). However, since the small scales are presumably more homogeneous and isotropic then the large scales, it should be possible to parametrize the small scales using simple and more general models. The simple approach applied to numerous LES calculations is the SGS turbulent Prandtl number ( $Pr_{SGS}$ ).

In the present paper the constant heat flux boundary condition was assumed, allowing nonzero wall temperature fluctuations and the effects of temperature fluctuations close to the wall are investigated using LES approach. The near wall range is resolved and subgrid-scale (SGS) turbulence model for non-unity Prandtl number by Otic [4] is applied to analyze forced convection in a channel at friction velocity-based Reynolds numbers of 390 and 599, for Prandtl numbers 0.701 and 0.022. Simulation data is statistically analyzed and compared with the DNS results from the literature. It is shown that temperature fluctuations are of great importance near the wall in both cases. Therefore, if the near wall region is approximated turbulence models must account for the temperature variance. A simple criteria for the contribution of turbulence models to the resolved scales in the entire computational domain is also provided.

### 1. Numerical method

# 1.1. Basic Equations

The governing equations for the velocity field are filtered Navier-Stokes and continuity equations

$$\frac{\partial \overline{U_i}}{\partial t} + \frac{\partial}{x_j} (\overline{U_i} \, \overline{U_j}) = -\frac{\partial \overline{p}}{\partial x_i} + \frac{\partial}{x_j} (\overline{S_{ij}} - B_{ij}),$$

$$\frac{\partial \overline{U_i}}{\partial x_i} = 0,$$
(1)

where bar denotes filtering,  $U_i$  is the velocity vector, p the pressure,  $S_{ij} = vD_{ij}$  the viscous stress tensor, v the molecular viscosity,  $D_{ij} = (\frac{\partial U_i}{\partial x_j} + \frac{\partial U_j}{\partial x_i})$  the strain rate tensor and  $B_{ij}$  the SGS tensor. The filtered temperature equation reads

$$\frac{\partial \overline{T}}{\partial t} + \frac{\partial \overline{U_j} \, \overline{T}}{\partial x_j} = \frac{\partial}{\partial x_j} \left( \kappa \frac{\partial \overline{T}}{\partial x_j} - q_j \right), \tag{2}$$

where T is the temperature and  $\kappa$  the thermal diffusivity. The scalar flux  $q_j$  represents transport of T due to turbulent scales too small to be resolved on the computational grid. Here the filtering operator  $\overline{F}$  denotes the average over the computational grid cell for any quantity F and  $f = F - \overline{F}$  the deviation thereof.

# 1.2. Subgrid-Scale Models

In this study we apply an eddy-viscosity SGS model to account for unresolved scales of the velocity field. This modeling is based on the hypothesis that the deviatoric part of the SGS stress tensor is locally aligned with the filtered deviatoric part of the strain rate tensor,

$$B_{ij} = 2/3K\mathbf{I} - \nu_{SGS}\overline{D_{ij}^{D}},$$

$$K = 1/2 \operatorname{tr}(B_{ij}), \quad \overline{D_{ij}^{D}} = \overline{D_{ij}} - 1/3\operatorname{tr}(\overline{D_{ij}})\mathbf{I},$$
(3)

where K is the SGS kinetic energy, **I** the unit tensor and  $v_{SGS}$  the SGS eddy viscosity. The transport equation for K can be derived by contracting the transport equation for  $B_{ij}$ . The closure problem is therefore, the determination of K and  $v_{SGS}$ . Assuming local equilibrium the modeled equation for K reads

$$\frac{\partial K}{\partial t} + \frac{\partial (\overline{U_j}K)}{\partial x_j} = -B_{ij}\overline{D_{ij}} + \frac{\partial}{\partial x_j}(v_{SGS}\frac{\partial K}{\partial x_j}) - C_{\varepsilon}\Delta^{-1}K^{3/2},\tag{4}$$

where  $v_{SGS} = C_V \Delta K^{1/2}$ ,  $\Delta$  is the filter width and  $C_V$ ,  $C_E$  are empirical coefficients. The dynamic procedure first introduced by Germano [5] can be applied to determine the coefficient  $C_V$ . This results in a dynamic one equation model (see e.g. Ghosal, Lund, Moin and Akselvoll [6] or Fureby, Tabor, Weller and Gosman [7]). In this study the dynamic one equation SGS model for the velocity field is used. This model provides for the proper asymptotic behavior of the stresses near the wall, and it vanishes in laminar flow without intermittency functions.

To close the energy equation (2),  $q_j$  must be modeled. A widely applied gradient diffusion model reads

$$q_j = -\kappa_{SGS} \frac{\partial \overline{T}}{\partial x_i},\tag{5}$$

with the turbulent eddy diffusivity  $\kappa_t$  defined as

$$\kappa_{SGS} = \frac{\nu_{SGS}}{Pr_{SGS}},\tag{6}$$

where  $Pr_{SGS}$  is the SGS turbulent Prandtl number. Based on one equation subgrid model for the velocity field and on the temperature and velocity spectra of the unresolved scales an one equation

The 14<sup>th</sup> International Topical Meeting on Nuclear Reactor Thermal Hydraulics NURETH-14 Toronto, Ontario, Canada, September 25-29, 2011

Test case	Pr	$Re_{ au}$	$Pr_{SGS}$	$N_1 \times N_2 \times N_3$
A	0.701	390	0.45	$120 \times 120 \times 96$
В	0.022	390	2.5	$120 \times 120 \times 96$
C	0.022	598	2.5	$140 \times 140 \times 140$

**Table 1**Test case summary

subgrid model for liquid metal forced convection is derived by Otic, [4]. The model provides an estimate for subgrid turbulent Prandtl number ( $Pr_{SGS}$ ) which accounts for effects of molecular fluid properties on the energy transfer at low to moderate Péclet numbers. The SGS heat flux model derived in [4] reads

$$\kappa_{SGS} = C_{v} (4\alpha/\beta)^{(1/2)} Pr^{(4/9)} \Delta K^{1/2}, \tag{7}$$

where the coefficients  $\alpha$  and  $\beta$  are determined from the experimental results and turbulence theory as

$$\alpha \sim 1.6, \quad \beta \sim 1.3,$$
 (8)

(see e.g. Monin and Yaglom [8] and Hinze [9]). For Pr=1 the equation (7) yields  $Pr_{SGS}=0.457$ . This SGS turbulent Prandtl number is close to the value 0.42 which is widely used for turbulent convection in air (see e.g. Deardorf [10]). For Pr=0.022 the SGS turbulent Prandtl number estimated using (7) is 2.495. The above equation together with the dynamic one-equation model introduced in the previous subsection represents the suggested SGS model for liquid metal forced convection. In the next section this approach is applied to simulate turbulent forced convection in a channel.

## 2. Simulation results and discussion

A relevant test case for examination of the LES results is the channel flow, where DNS and experimental data are available for comparison. In this study two cases of passive scalar transport in turbulent channel flow are performed for Prandtl numbers 0.701 and 0.022 at friction velocity based Reynolds numbers  $Re_{\tau}=390$  and 598 (see Table 1). The channel is confined with two parallel plates 2h apart, where h is the channel half-width. The computational domain for both cases is  $6h \times 2h \times 3h$  in the streamwise, cross-stream and spanwise directions, respectively. The flow is driven by a fixed mass flow rate in the streamwise direction. No-slip conditions are used at the walls while the periodic boundary conditions are applied on other boundaries. Constant wall heat flux of  $20 \ W/m^2$  is considered at both walls while the initial temperature of wall and fluid is chosen as  $500^{\circ} K$ . The filtered equations are discretized using the finite volume method. The algorithm is second order accurate both in space and time and the governing equations are considered in the dimensional form. Time step is specified based on the requirement that maximum Courant number (Co) is below 0.5. The system of algebraic equations is solved by an incomplete Choleski conjugate gradient method and the predictor-corrector PISO scheme for pressure is applied. The calculations presented here are performed using the OpenFOAM CFD toolbox, see e.g. Weller et

al. [11]. The initial isothermal constant velocity field was integrated in time until the fully developed state is reached. Subsequently the computations are carried out until the passive scalar fields reached statistically steady states. For the cases A and B the initial velocity field is introduced from the previous calculation and the passive scalar is introduced independently for both cases.

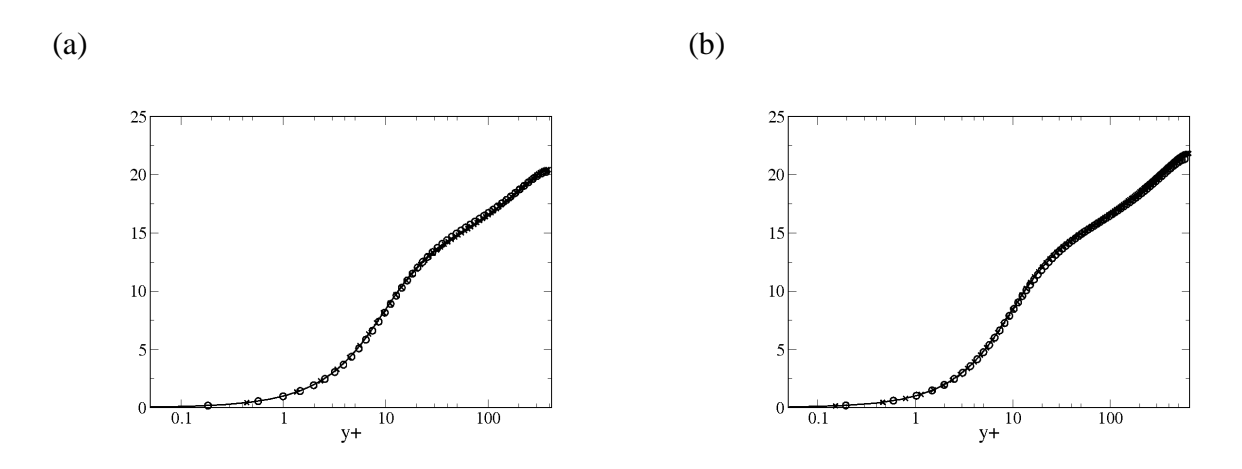


Fig. 1: Mean velocity. (a)  $Re_{\tau} \sim 390$ : —, DNS MKM; ×, DNS KAM;  $\circ$ , LES case A. (b)  $Re_{\tau} \sim 600$ : —, DNS MKM; ×, DNS AKM;  $\circ$ , present LES case C.

Statistical results are normalized by the friction velocity  $u_{\tau}$  and and the wall surface heat flux  $T_{\tau} = (\kappa \frac{\partial \langle T \rangle}{\partial y}|_{w})/u_{\tau}$ . Throughout the paper the superscript + assign a non-dimensional quantity scaled by wall variables e.g.  $y^{+} = yu_{\tau}/v$  and  $T^{+} = \langle T \rangle/T_{\tau}$ . To compare with the DNS data the mean temperature profile is considered as  $\langle T \rangle|_{w} - \langle T \rangle$ .

Kawamura et al. [3], hereafter KAM, and Abe et al. [12], hereafter AKM, performed DNS of turbulent heat transfer in channel flow at  $Re_{\tau} = 395$  and 640 for both Pr = 0.71 and 0.025. In these simulations passive scalar is introduced as the ideal isoflux heat BC from both walls. These and isothermal DNS data for  $Re_{\tau} = 395$  and 590 by Moser *et al.* [13], hereafter MKM, are also used for comparisons. To evaluate the present LES results the mean velocity profile and root-mean-square (rms) values are shown and compared with the DNS results by Moser *et al.* [13], Kawamura *et al.* [3], and Abe *et al.* [12]. The LES results for the mean velocities are in very good agreement with DNS, Fig. 1. Because of the higher Reynolds number the results of Abe *et al.* [12] differs slightly in the channel central region as compared to the DNS results by Moser *et al.* [13] and to the present LES (case C, Fig. 1 b).

In figure 2 velocity root-mean-square (rms) values evaluated from the LES are presented and compared with the DNS results. Figure 2 indicate a very good agreement of the LES results with the DNS. However, for  $Re_{\tau} \sim 600$  there is a small discrepancy for  $u_{1RMS}$  in the range  $y^+$  of 100-300 compared to the results by Moser *et al.* [13], figure 2 (b). Because of the higher Reynolds number the results of Abe *et al.* [12] are slightly different then the DNS by Moser *et al.* [13] and the present LES, figure 2 (b).

In the following we present a criteria for the SGS model contribution. This simple criteria allows

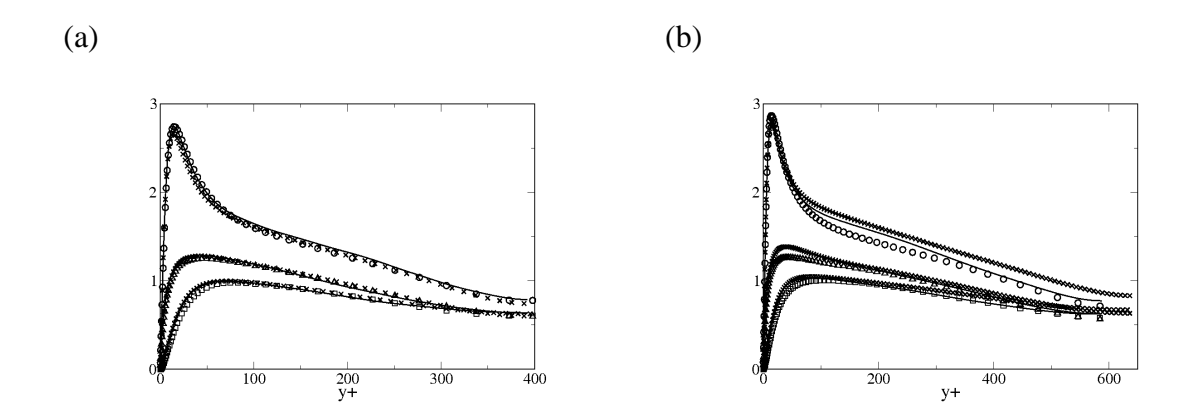


Fig. 2:  $u_{iRMS}$ . (a)  $Re_{\tau} \sim 390$ : —, DNS MKM; ×, DNS KAM; Present LES, case A:  $\circ$ ,  $u_{1RMS}$ ;  $\triangle$ ,  $u_{2RMS}$ ;  $\square$ ,  $u_{3RMS}$ . (b)  $Re_{\tau} \sim 600$ : —, DNS MKM; ×, DNS AKM; Symbols represent the same as in a) for present LES, case C.

an iterative simulation procedure where the level of approximation can be adjusted. Here the governing equations (1) and (2) are solved in the dimensional form using constant fluid properties. Since turbulent eddy viscosity and turbulent eddy diffusivity modeling is applied, (equations (1) - (5)), a simple rearrangement of the viscosity and diffusivity terms yields

$$v\left(1 + \frac{v_{SGS}}{v}\right),$$

$$\kappa\left(1 + \frac{\kappa_{SGS}}{\kappa}\right).$$
(9)

The dimensionless ratios  $(v_{SGS}/v)$  and  $(\kappa_{SGS}/\kappa)$  provide a simple criteria for the contribution of SGS turbulence models in the entire computational domain. It is a simple measure for the contribution of SGS models to the resolved scales. Main advantages are: a) no sophisticated post-processing is required as e.g. data filtering over some wave number range; b) the local spatial resolution is evaluated over every computational cell without additional computations.

The discussion on spatial resolution requirements is carried on over the last fourty years. However, apart of few well established integral criteria like  $Re^{9/4}$  for the resolution of the Kolmogorov scale, there is still no general a priori estimate for local mesh resolution (although some attempts are done). The reason is plausible; there is no general geometry, no general mesh structure, no universal turbulence model and no universal scaling law.

Applying the criteria (9) an iterative simulation procedure is presented in the following. Using this procedure a simulation can be performed at a chosen level of approximation. The procedure reads:

- 1. Estimate coarse mesh using some integral criteria (e.g.  $Re^{9/8}$  resolution requirement for the inertial subrange) and define the flow-through time (e.g. Rayleigh-Bénard case is different from pipe flow),
- 2. Generate mesh and perturb initial velocity field,

- 3. After two flow-through times evaluate criteria (9),
  - a) If sharp peaks exist in the fields of  $(v_{SGS}/v)$  and  $(\kappa_{SGS}/\kappa)$  restructure the mesh to avoid them,
  - b) Else, continue,
- 4. Refine the mesh so that the local maxima of  $(v_{SGS}/v)$  and  $(\kappa_{SGS}/\kappa)$  are below your level of approximation (e.g. in this case the contribution of SGS model is chosen to be less then 10%, see the following discussion),
- 5. Interpolate previous results to the finer mesh,
- 6. After two flow-through times evaluate the averaged criteria (9),
  - a) If sharp peaks exist go to 3. and repeat the steps.
  - b) If the required level of approximation is not satisfied go to 4. and repeat the steps.
  - c) Else, continue.

For non-buoyant flow scalar transport is first introduced at the procedure step 6. c). In general, profiles of  $(v_{SGS}/v)$  and  $(\kappa_{SGS}/\kappa)$  should be smooth functions. Steep gradients in the proximity of the local maxima (or minima) indicate inadequate mesh structure which should be corrected. Apart of the criteria check, the procedure steps 1., 2., 4. and 5. are essentially common simulation practice. The main advantage of this procedure is that no additional computational costs are introduced.

Figure 3 show the distribution of the averaged criteria (9) after forty flow-through times. It is worth to notice that no significant difference between the averaged criteria after two and after forty flow-through times could be observed for these simulations. Figure 3 (a) shows the smooth distribution of the averaged criteria  $\langle v_{SGS} \rangle / v$  for LES cases B and C. The maximum contribution of the SGS model do not exceed 7%. This indicates that LES cases are well posed. The figure 3 (a) also indicate correct vanishing behavior of the dynamic one equation model in the near wall region. The number of mesh cells in the DNS by Kawamura  $et\ al.$  [3] for  $Re_{\tau}\sim 395$ , is about 8.4 million where the present LES use about 1.4 million cells, see table 1. The DNS by Abe et al. [12],  $Re_{\tau}=640$ , is fourth order accurate very high resolution simulation in the  $12.8\times 2\times 6.4$  box. The number of mesh cells used in this DNS ([12]) is about 248 million where 256 grid points between the walls are used. The number of mesh cells used in the present LES case C is about 2.7 million where 140 grid points between the walls are used, see table 1.

Figure 3 (b) shows the smooth distribution of the averaged criteria  $\langle \kappa_{SGS} \rangle / \kappa$  for LES cases *B* and *C*. The maximum contribution of the SGS model to the temperature field is about 0.06% at  $y+\sim 10$ , i.e. negligibly small. Liquid metal convection is characterized by large thermal diffusivity compared to the molecular viscosity i.e. small Prandtl number  $Pr = \nu / \kappa$ . Hence, the small scale energy spectra of the temperature field decays much faster than the energy spectra of the velocity field and the temperature field is dominated by the large scale motion. Therefore, it is almost obvious that for Pr << 1 follows  $Pr_{SGS} > 1$ , see e.g. Tennekes and Lumley [14]. Modeling approach applied here estimates  $Pr_{SGS} \sim 2.5$ , see table 1. An arbitrary setting of  $Pr_{SGS} = 1$  will increase the maximum contribution of the SGS model to the temperature field to 0.15%, i.e. still

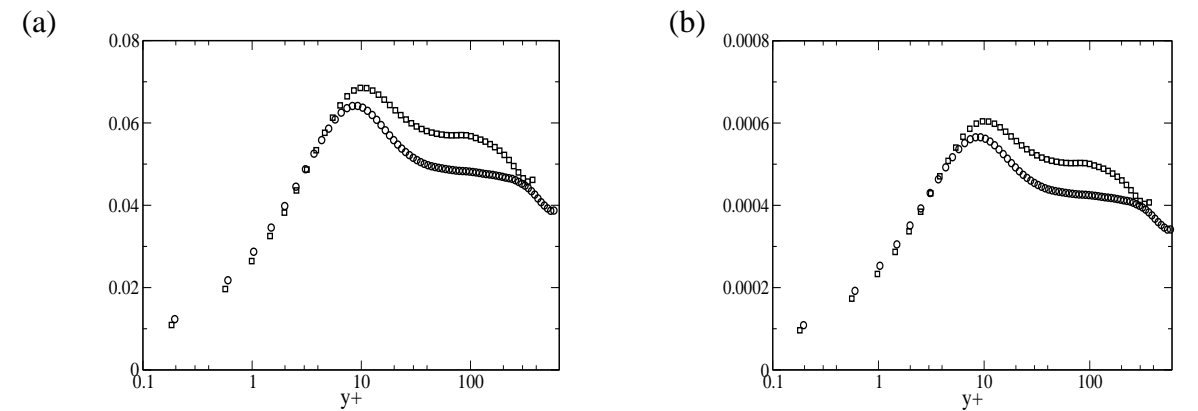
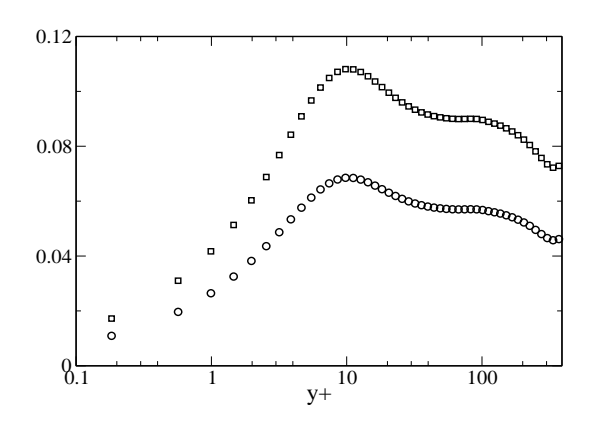


Fig. 3: (a)  $\langle v_{SGS} \rangle / v$ :  $\Box$ , LES case B;  $\circ$ , LES case C. (b)  $\langle \kappa_{SGS} \rangle / \kappa$ :  $\Box$ , LES case B;  $\circ$ , LES case C.

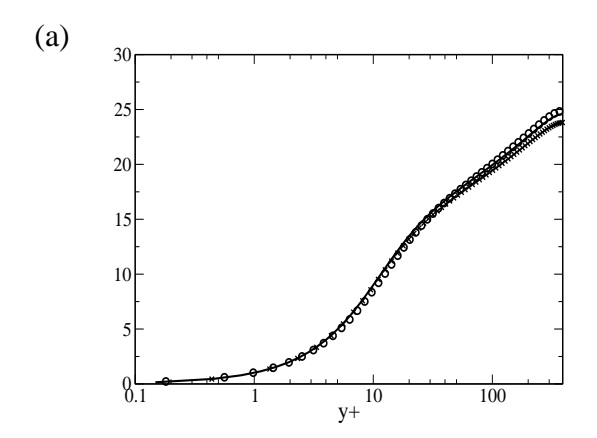


**Fig. 4**:  $Re_{\tau} \sim 390$ , LES case A:  $\bigcirc$ ,  $\langle v_{SGS} \rangle / v$ ;  $\square$ ,  $\langle \kappa_{SGS} \rangle / \kappa$ .

negligibly small. Since the turbulence model show correct near wall and overall behavior and introduces negligibly small computational costs for the calculations of the temperature field as compared to the overall simulation costs, there is no need to switch it off even for these low Péclet number cases  $(Pe_{\tau} = Re_{\tau} \times Pr)$ . Figure 4 shows the distribution of the averaged criteria  $\langle v_{SGS} \rangle / v$  and  $\langle \kappa_{SGS} \rangle / \kappa$  for the LES case A. The maximum contribution of the SGS model to the temperature field is about 11% at  $y+\sim 10$ .

For comparison of the temperature fields two sets of DNS data for  $Re_{\tau} \sim 390$  are used. Kawamura et~al.~[3] performed second order accurate DNS in the  $6.4 \times 2 \times 3.2$  box with the resolution of  $256 \times 128 \times 256$  mesh points. In the same group, fourth order accurate very high resolution DNS in the  $12.8 \times 2 \times 6.4$  box with the resolution of  $512 \times 192 \times 512$  for the same  $Re_{\tau} = 395$  and Pr = 0.71 was performed, see Abe et~al.~[12]. The mean temperature profiles for  $Pr \sim 0.7$  and 0.022 as ratio  $T^+/Pr$  are given in Fig. 5 (a) and (b), respectively.

For the case  $Pr \sim 0.7$  the LES mean temperature profiles are nearly identical with the second order accurate DNS despite the different thermal boundary conditions, Fig. 5 (a). It is found that the mean temperature profile does not depend on the type of the boundary condition. These results are



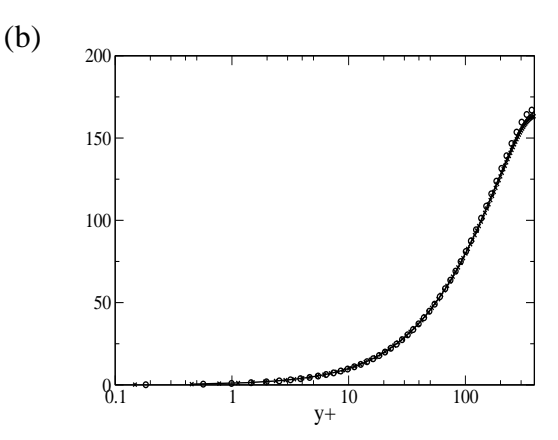


Fig. 5:  $T^+/Pr$ . (a)  $Pr \sim 0.7$ : —, DNS KAM;  $\times$ , DNS AKM;  $\circ$ , LES case A. (b)  $Pr \sim 0.022$ : —, DNS KAM;  $\times$ , DNS AKM;  $\circ$ , LES case B.

consistent with the results by Tiselj *et al.* [2] for  $Re_{\tau} \sim 180$  and Pr = 1. The fourth order accurate DNS [12] indicates slightly lower mean temperature at  $y^+$  above 300, Fig. 5 (a). For the case  $Pr \sim 0.022$  similar behavior can be observed. However, the discrepancy between second to the forth order accurate simulations is very small.

Figure 6 shows normalized temperature rms values  $\theta_{rms}^+/Pr$ . In addition to the second and forth order accurate DNS data by [3] and [12] also the DNS results by Tiselj *et al.* [2] and Kawamura *et al.* [3] for  $Re_{\tau} \sim 180$  and Pr = 1 are included for comparison, figure 6 (a). In figure 6 (a) results by Kawamura *et al.* [3] (dashed line) are compared with the results by Tiselj *et al.* [2] (squares) for  $Re_{\tau} \sim 180$ . LES results (circle) and DNS results (× and straight line) for  $Re_{\tau} \sim 390$  are also compared in the figure 6 (a). The main difference is observed for temperature rms near the wall. Temperature fluctuations retain a nonzero value on the wall for isoflux boundary condition. Apart of the thermal boundary layer no influence of different BC can be observed. The fourth order accurate DNS [12] indicates slightly higher  $\theta_{rms}^+$  at  $y^+$  around 20. In figure 6 (b) LES results (circle) are compared with DNS results (× and straight line) for  $Pr \sim 0.022$ . The same effect as in the case  $Pr \sim 0.7$  can be observed, i.e. the temperature fluctuations retain a nonzero on the wall for isoflux boundary condition. The discrepancy between second and forth order DNS is more pronounced in this case, figure 6 (b).

The normalized mean temperature profiles  $T^+/Pr$  for  $Re_{\tau} \sim 600$  and  $Pr \sim 0.022$  are presented in Fig. 7 (a). the mean temperature profile does not depend on the type of the boundary condition also in this case. However, small discrepancy between second order accurate LES and forth order accurate DNS can be observed in the center of the channel. This difference is similar to the differences observed for  $Re_{\tau} \sim 390$  also between DNS results, see Fig. 6 (b).

Fig. 7 (b) show normalized  $\theta_{rms}^+/Pr$  profiles for the same cases. Temperature fluctuations retain a nonzero value on the wall for isoflux boundary condition also in this case. The differences between LES and DNS results at the edge and apart of the thermal boundary layer are here more pronounced. However, this difference is not only due to different order of accuracy or numerical approach (DNS apply finite difference while LES apply finite volume) but also due to the different Péclet number  $Pe_{\tau} = Re_{\tau} \times Pr$ . The DNS Péclet number is  $Pe_{\tau} = 16$  where for LES  $Pe_{\tau} = 13.156$ .

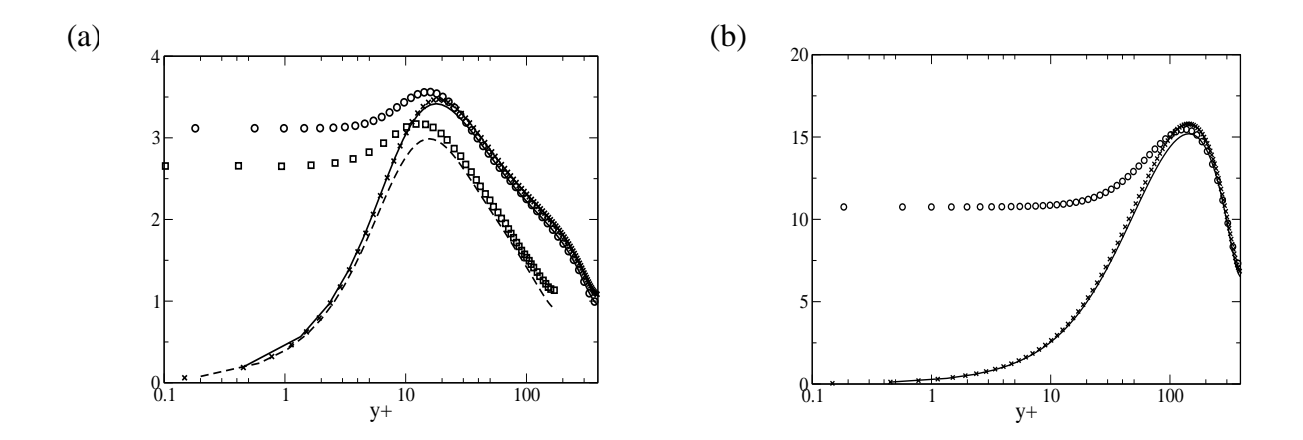


Fig. 6:  $\theta^+_{rms}/Pr$ . (a)  $Pr \sim 0.7$ : —, DNS KAM;  $\times$ , DNS AKM; - - -, DNS KAM;  $\square$ , DNS Tiselj etal.;  $\circ$ , LES case A. (b)  $Pr \sim 0.022$ : —, DNS AKM;  $\times$ , DNS KAM;  $\circ$ , LES case B.

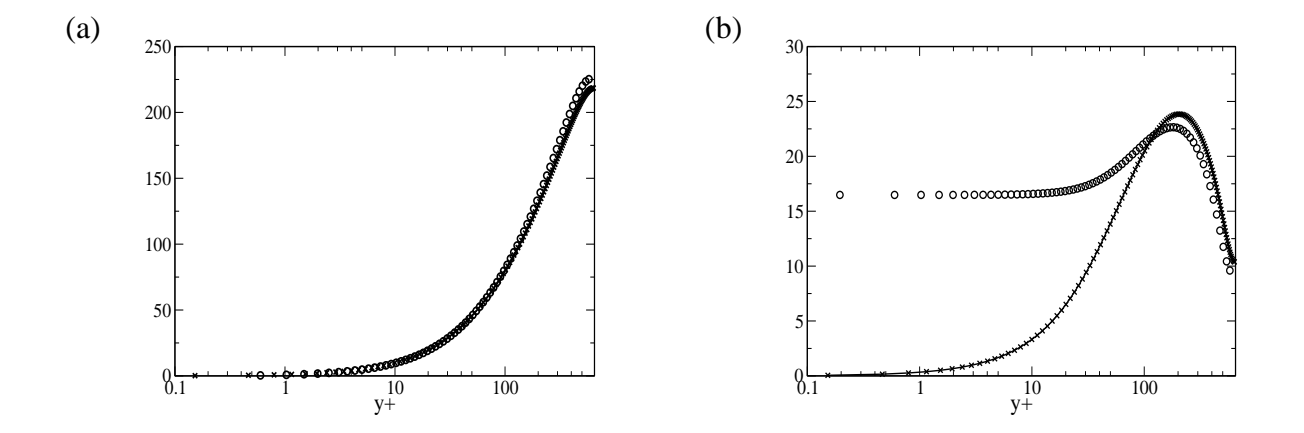


Fig. 7:  $\circ$ , LES case C;  $\times$ , DNS KAM; for (a)  $T^+/Pr$  and (b)  $\theta_{rms}^+/Pr$ .

## 3. CONCLUSIONS

In the present paper the constant heat flux boundary condition was assumed, allowing nonzero wall temperature fluctuations and the effects of temperature fluctuations close to the wall are investigated using LES approach. For practical calculations this type of boundary conditions is required since the assumption of zero temperature fluctuations at the walls can not explain the wall thermal streaks. The near wall range is resolved and subgrid-scale (SGS) turbulence model for non-unity Prandtl number by Otic [4] is applied to analyze forced convection in a channel at  $Re_{\tau} = 390$  and 598, for Prandtl numbers of 0.701 and 0.022. Simulation data is statistically analyzed and compared with the DNS results from the literature. It is shown that temperature fluctuations are of great importance near the wall in both cases. Therefore, if the near wall region is approximated turbulence models must account for the temperature variance. However, there is no influence of the boundary conditions on the temperature variance profiles in the center of the channel. No influence of heat flux boundary conditions on mean temperature profiles was observed. The results are consistent with the results reported in the literature. A simple criteria for the contribution of turbulence models to the resolved scales in the entire computational domain is also provided. Additional ongoing LES for  $Re_{\tau} = 1450$  at Pr = 0.022 will be presented at the conference.

# **ACKNOWLEDGMENT**

This work received financial support by the EU within the integrated project THINS under the contract number FI6W-CT-2004-516520.

#### REFERENCES

- 1. T. P. Sommer, R. M. C. So, and H. S. Zhang. Heat transfer modeling and the assumption of zero wall temperature fluctuations. *Trans. ASME, J. Heat Transfer*, 116(4):855–863, 1994.
- 2. Iztok Tiselj, Elena Pogrebnyak, Changfeng Li, Albert Mosyak, and Gad Hetsroni. Effect of wall boundary condition on scalar transfer in a fully developed turbulent flume. *Physics of Fluids*, 13(4):1028–1039, 2001.
- 3. H. Kawamura, H. Abe, and Y. Matsuo. DNS of turbulent heat transfer in channel flow with respect to reynolds and prandtl number effects. *International Journal of Heat and Fluid Flow*, 20(3):196 207, 1999.

4.

- 5. M. Germano. Turbulence: the filtering approach. J. Fluid Mech., 238:325.336, 1992.
- 6. S. Ghosal, T.S. Lund, P. Moin, and K. Akselvoll. A dynamic localization model for large-eddy simulation of turbulent flows. *J. Fluid Mech.*, 286:229–255, 1995.
- 7. C. Fureby, G. Tabor, H.G. Weller, and A.D. Gosman. A comparative study of subgrid scale models in homogeneous isotropic turbulence. *Phys. Fluids*, 9:1416–1429, 1997.
- 8. A. S. Monin and A. M. Yaglom. *Statistical Fluid Mechanics*. MIT Press, Cambridge, MA, 1971.
- 9. J.O. Hinze. Turbulence. McGraw-Hill, 2 edition, 1975.
- 10. J.W. Deardorff. Investigation of turbulent thermal convection between horizontal plates. *J. Fluid Mech.*, 28:675–704, 1967.
- 11. H.G. Weller, G. Tabor, H. Jasak, and C. Fureby. A tensorial approach to computational con-

- tinuum mechanics using object orientated techniques. *Computers in Physics*, 12:620–631, 1998.
- 12. H. Abe, H. Kawamura, and Y. Matsuo. Surface heat-flux fluctuations in a turbulent channel flow up to re[tau]=1020 with pr=0.025 and 0.71. *International Journal of Heat and Fluid Flow*, 25(3):404 419, 2004.
- 13. R. D. Moser, J. Kim, and N. N. Mansour. Direct Numerical Simulation of turbulent channel flow up to  $Re_{\tau} = 590$ . *Phys. of Fluids*, 11:943–945, 1999.
- 14. H. Tennekes and J.L. Lumley. A first course in turbulence. MIT press, 1972.